Small 14.21 (2018): 1800633

DOI: https://doi.org/10.1002/smll.201800633

Unprecedented Centimeter-long Carbon Nitride Needles: Synthesis, Characterization and Applications

Jesús Barrio, [†] *Lihua Lin,* [¥] *Pilar Amo-Ochoa,* [‡] *Jonathan Tzadikov,* [†] *Guiming Peng,* [†] *Jingwen Sun,* [†] *Félix Zamora,* [‡§] *Xinchen Wang,* [¥] *Menny Shalom* [†]*

Jesús Barrio, Jonathan Tzadikov, Dr. Guiming Peng, Dr. Jingwen Sun, Prof. Menny Shalom. † Department of Chemistry, Ben Gurion University of the Negev, Beersheba 009728, Israel E-mail: mennysh@post.bgu.ac.il

Ling Lihua, Prof. Xinchen Wang.

¥ College of Chemistry, Fuzhou University, Gong Ye Road 523, Fuzhou, Fujian, Fuzhou 350002 P. R. China.

Dr. Pilar Amo-Ochoa, Dr. Félix Zamora.
‡ Departamento de Química Inorgánica, Institute for Advanced Research in Chemical Sciences (IAdChem) and Condensed Matter Physics Center (IFIMAC), Universiidad Autónoma de Madrid, E-28049 Madrid, Spain

§ Instituto Madrileño de Estudios Avanzados en Nanociencia (IMDEA-Nanociencia), Cantoblanco, E-28049 Madrid, Spain

Keywords: one-dimensional (1D) nanostructures, polymeric carbon nitride, direct electric measurements, photocatalysis

Free standing centimeter-long one-dimensional (1D) nanostructures are highly attractive for electronic and optoelectronic devices due to their unique photophysical and electrical properties. Here we report on a simple, large-scale synthesis of centimeter-long 1D carbon nitride (CN) needles with tunable photophysical, electric and catalytic properties. Successful growth of ultra-long needles is acquired by the utilization of 1D organic crystal precursors comprised of CN monomers as reactants. Upon calcination at high temperatures, the shape of the starting crystal is fully preserved while the CN composition and porosity as well as optical and electrical properties can be easily tuned by tailoring the starting elements ratio and final calcination temperature. The facile manipulation and visualization of the CN needles endow their direct electrical measurements by placing them between two conductive probes. Moreover, the CN

needles exhibit good photocatalytic activity for hydrogen production owing to their improved light harvesting properties, high surface area and advantageous energy bands position. The new growth strategy developed here may open opportunities for a rational design of CN and other metal-free materials with controllable directionality and tunable photophysical and electronic properties, toward their utilization in (photo)electronic devices.

1. Introduction

The fabrication of free-standing centimeter-long one dimensional (1D) nanostructures as carbon nanotubes [1-3] and other semiconductors [4] has attracted a lot of attention in recent years due to the introduction of new feasible applications owing to the combination of the unique properties and macroscopic scale of these nanostructures. Their intriguing mechanical, electronic and optical properties, [5] as well as their processability, have allowed their exploitation in many fields such as photocatalysis, [6] electronic devices, [7] sensors [8] and solar cells. [9] Moreover, the ultra-long size of the self-standing 1D materials permit their straightforward utilization in (photo)electronic devices [10, 11] due to their easy visualization and manipulation. For example, the electronic properties (i.e. conductivity) can be easily extracted by a direct electrical measurement. The exceptional properties of 1D semiconductors-based photocatalysts were proven as highly beneficial due to the facile charge carrier separation and transport which leads to low charge recombination thanks to reduced grain boundaries and charge directionality.[12, 13] Polymeric graphitic carbon nitride (CN) has emerged as a highly promising low cost metal free material [14-18] due to its outstanding electronic properties, which have been exploited in various applications – including in photo- and electro-catalysis, [19-22] heterogeneous catalysis, [23] CO_2 reduction, [24] water splitting, [25-27] light-emitting diodes [28], and PV cells [29, 30]. CN comprises only carbon and nitrogen, and it can be synthesized by several routes. The traditional CN synthesis entails the solid-state condensation of C/N monomers (dicyanamide, melamine and urea to name a few) at high temperatures. The solid-state reaction

often results in rather unordered materials with large grain boundaries and low photoactivity. To circumvent the abovementioned limitations, a great progress was acquired by introducing heteroatoms and molecules within CN structure [31-34] developing new exfoliation techniques [25, 26] and by utilizing hard and soft templating methods [37, 38]. Recently, our group and others showed that by the rational design of CN monomers a great control of their chemical, photophysical and catalytic properties can be achieved [39-45]. Several successful approaches were suggested for 1D CN growth. However, these methods lie on the use of templating agent, metal as co-catalyst and are limited to the growth of CN with maximum micron size [46-49].

Here we report on the large-scale and facile synthesis of self-standing centimeter-long carbon nitride needles with controllable optical properties, porosity and composition by utilizing 1D organic crystals as precursor. The single crystals were prepared by using melamine, benzoguanamine and hydrochloride acid. Upon calcination, the macrostructure was precisely preserved and parameters as porosity, photophysical and catalytic activity can be tuned by calcination temperature and the elements ratio within starting crystal. The advantages of the centimeter-long needles are exemplified here by direct conductivity measurements of CN for the first time and by a great enhancement of their photoactivity.

2. Results and discussion

The molecular structure of the melamine needle-shaped crystals (M-nsc) was determined by single crystal X-ray diffraction analysis (SC-XRD). The unit cell parameters are provided in Figure S1-S2, revealing a melaminium chloride hemihydrate structure, [50] where the protonated melaminium cations lie on a twofold axis and the chloride anions and water molecule lie on the *m* plane. The melaminium residues are interconnected by N-H···N hydrogen bonds, forming chains parallel to the (001) plane. A three-dimensional network is formed through hydrogen-bond interactions with chloride anions and water molecules. Further evidence for the formation of an organic single crystal is given by FT-IR spectroscopy, XRD measurements and XPS

analysis (Figure S3 - S4). The new interaction within the crystal leads to the disappearance of the stretching bands of the amine groups (νNH_2) at 3463 and 3419 cm^{-1} and to a general shift to lower wavenumbers of the main melamine vibrations due to intramolecular interactions; carbon-nitrogen stretching mode (νCN) from 1527-1426 to 1490-1342 cm^{-1}, ring deformation bands from 1192-1020 to 1158-1000 cm^{-1} and the breathing ring vibration from 807 to 773 cm^{-1}. [51] Powder X-ray diffraction (PXRD) measurements show a well-resolved peak at 10.5° which indicates the formation of an ordered material with a consistence repeating unit in plane (Figure S3b). As well another strong evidence for the new arrangement is provided by the enhancement of the absorption optical density of the crystal compared to melamine powder, owing to better pi-pi interactions (Figure S3c) [52]. XPS analysis further confirmed the strong reorganization of melamine molecules in the presence of Cl anions (Figure S4, further discussion is given in the SI). SEM images of the crystals show up to couple millimeters long needle with several tens of microns' width and a flat surface (Figure 1).

Photoactive CN materials were obtained by the calcination of the needle-shaped crystals at different temperatures (500, 600 and 650 °C) for 4h under a nitrogen atmosphere. It is necessary to highlight the fact that the needle shape of the melamine crystal along with its size was preserved upon heating to 650 °C as shown later in this paper. The condensation progress of the crystals into CN materials can be followed by TGA (Figure S5). The hydrogen-halogen interaction in the single crystal strongly quenched the known degradation and sublimation of melamine at high temperatures. The condensation of melamine occurs in one pronounced step with a significant weight loss of 85% at around 400 °C while the melamine crystal condensate in several steps, resulting in high reaction yield. The first weight loss (4%) takes place at ~120 °C owing to the release of H_2O. Subsequently, at higher temperature (from ~250 to 450 °C) the crystal turns into CN and around 40% of the material remains at 600 °C.

FT-IR and XRD (Figure S6) measurements prove the formation of CN materials after calcination. The analysis shows the typical stretching modes of CN heterocycles from 1200 to 1600 cm^{-1} and the breathing mode of triazine units at 800 cm^{-1} in all of the materials. The general reduced peaks intensity of the specie calcined at 650 °C indicates a weakened vibration of the tri-s-triazine due to the partial loss of N atoms from CN structure. The typical (100) and (002) crystal planes of CN at 13.6 and 27.3° can be observed from the XRD patterns of the materials calcined at 500 and 600 °C. At 650 °C the intensity was significantly quenched due to partial degradation of the tri-s-triazine units. The structural cleavage occurs mainly by the removal of N atoms, mainly from the surface as shown by Elemental Analysis, Table S1.

SEM images of CN materials after calcination (Figure 2) at different temperatures unveiled that the needle-shape of the starting crystals was preserved upon heating and centimeter long porous needles can be obtained (Figure S7). All the materials demonstrate an ordered layered structure and the morphology changes from porous framework along the needle at 500 °C to hollow cavities at 600 and 650 °C.

Nitrogen-sorption measurements indicated that the porosity increased at higher calcination temperatures (Figure S8) and the surface areas inclined from 15 $m^2 g^{-1}$ to 99 and 185 $m^2 g^{-1}$ for the CN_{500}, CN_{600} and CN_{650}, respectively. We note that these values are impressive considering that no template or harsh chemical treatment were used. The layered structure of the materials is also evident by TEM images (Figure S9) where micrometer length sheets were observed. In order to elucidate the chemical and electronic properties of the CN materials, we performed XPS measurements (Figure 3). For CN_{500} and CN_{600} no big difference can be noticed. The C1s binding energies show a main carbon specie at 288.2 eV corresponding to a C-N-C coordination and two smaller contributions at 286.2 and 284.8 that belong to adventitious C-O-C and C-C species, respectively. In the N1s spectrum, several binding energies corresponding to C-N=C groups (398.7 eV), $N-(C)_3$ (399.9 eV), C-N-H groups (401.3 eV) and to charging effects (404.2 eV) were detected. For CN_{650}, the C1s spectra revealed that the weight percentage of the C-N-

C specie (287.8 eV) decreased compared to the contribution of C-C bond (284.7 eV), confirming the slight degradation of the tri-s-triazine structure. As well, a new peak appears at 285.6 eV, which belongs to the formation of a new C=C π bond. [53] The N1s spectra revealed that the atomic weight percentage of the C-N=C species (398.5 eV) was considerably decreased compared to $N-(C)_3$, suggesting that the loss of nitrogen atoms occurs at the two-coordinated lattice sites. [54-56] The chemical species that belong to N-H groups (400.9 eV) and charging effects in heptazine rings (403.5 eV) can also be found. These results strongly support the formation of N vacancies in the CN_{650}.

The optical properties of the CN materials were evaluated by photo-physical measurements (Figure 4a, b). The absorption spectra of CN_{600} and CN_{650} were red-shifted compared to CN_{500}. The latter can be attributed to the creation of two different semiconducting domains or to enhanced amount of surface defects. [57] We assume that due to the large surface to bulk ratio the outer part of the needles reacts differently from the inner part leading to two different domains, where the outer shell is composed from slightly degraded tri-s-triazine units with N vacancies and the inner by intact tri-s-triazine units as confirmed by XPS measurements (Figure 4d). Photoluminescence (PL) spectroscopy is a very useful and sensitive technique for detecting electronic changes such as surface states in semiconductors. We observed that at high calcination temperatures the emission of the material was quenched, further supporting the two domains formation. Tauc Plot and Mott Schottky measurements disclosed that the conduction and valence band edges are suitable for water splitting reaction (Figure S10). We note that due to the formation of different semiconducting domains in the CN_{650} we couldn't obtained a reliable value.

In order to evaluate the photoactivity of the CN materials, we measured the hydrogen evolution in a water/triethanolamine (TEOA) solution (Figure 5a), with Pt as the cocatalyst, under a white-light illumination. CN_{650} demonstrated the highest catalytic activity (23 μmol H_2/h). Due

to the creation of two different semiconducting domains with different amount of N vacancies, and the appearance of a new adsorption band at 500 nm, we measured the quantum yield (QY) of CN_{650} under 420 and 490 nm illumination. The QY was found to be 1.0 and 0.5% at 420 and 490 nm, respectively. These values are relatively high considering that melamine was the only monomer used in the synthesis and that usually C/N materials are not active under illumination at 490 nm. The photoactivity of the CN materials was further tested by measuring the RhB dye degradation as a function of time under white light illumination. Amid the materials calcined at different temperatures, the CN_{650} showed superior photodegradation performance and the dye was fully degraded after 20 min. (Figure 5b). To elucidate the mechanism of RhB degradation, we measured the CN_{650} photodegradation in the presence of a hole scavenger and electron acceptor (TEOA and $AgNO_3$, respectively) and under N_2 or O_2 environment (Figure S11). The TEOA addition and N_2 purging resulted in a decline of the photodegradation process whilst flushing with O_2 or adding Ag^+ improved the photodegradation rates. These results strongly suggest that the photodegradation process occurs *via* photogenerated holes.

An enhanced photocatalytic activity could be due to several factors: better light harvesting (more charge carriers), better charge separation and larger surface area providing more amount of catalytic sites. Having all data in hand, we can conclude that all the three options are synergistically contributed to the photoactivity. The CN_{650} exhibits very high surface area and good light harvesting properties and the unique 1D structure allows better charge separation and transport. Upon calcination, in situ heterojunction can be formed, comprising of two semiconductors as discussed before. Besides the enhanced photocatalysis, the projection of the 1D crystal morphology and macrostructure into the final CN material opens the possibility to measure directly the conductivity of the needle-shape materials by contacting them between two graphite electrodes (Scheme S1) and recording the electrical current while applying a voltage from -10 to 10V. Due to the formation of many defects at high calcination temperatures

alongside the high surface area obtained in the materials, here we measured only CN_{500}. However, the large band gap resulted in a low conductivity (7.8 10^{-9} S cm^{-1}, Figure S12). In order to further increase the conductivity while preserving a flat and dense structure we doped the melamine needles with a carbon-rich molecule, namely BGA (2, 4-diamino-6-phenyl-1, 3, 5-triazine). The higher carbon amount in the precursor leads to enhanced carbon amount in the final CN already after calcination at 500 °C. FT-IR and XRD characterization of the needle-shaped crystals doped with BGA after their calcination at 500 °C (CN-BGA_x) confirmed the formation of modified-CN materials (Figure S13). Optical characterization indicated the narrowing of the materials band gap with increasing amount of dopant, ranging from 2.68 eV (pristine CN_{500}) to 2.45 eV for the CN-$BGA_{0.2}$ (Figure S14). SEM images of CN-BGA_x prove that the insertion of BGA within the CN reduced the voids throughout the 1D structure (Figure S15). The conductivity values (σ) of CN-BGA_x are enhanced compared to CN_{500}; from 7.8 10^{-9} S cm^{-1} to 2.5 10^{-7} S cm^{-1} for CN-$BGA_{0.2}$ (Figure 5c). Those values are in good agreement with the semiconductor behavior of CN materials and confirm that their charge carrier transport can be modulated by tailored design of the molecular crystal.

3. Conclusions

In summary, we demonstrated an efficient, scalable and straightforward method to synthesize centimeter-long carbon nitride 1D materials with a controllable photophysical, electronic and catalytic properties. The growth was acquired by the rational design of 1D organic crystal comprised of carbon nitride monomers. Upon condensation at high temperatures, the organic crystals shape can be fully preserved while the porosity as well as the optical and conductivity properties can be easily tuned by the calcination temperature and starting elements composition. The centimeter-long CN needles exhibit good photoactivity for hydrogen production owing to the enhanced light harvesting properties, high surface area, improved charge transport properties and favorable energy bands structure. We demonstrate that the use of centimeter-

long CN endows their direct electrical measurements, as well, a tailored design of the organic single crystal allows the modification of the electronic properties of the final CN materials by insertion of carbon-rich monomers leading to narrower band gaps and improved conductivity. We believe that this simple growth strategy of centimeter-long carbon nitride needles could be easily extended to grow other metal-free materials with controllable directionality and tunable photophysical and electronic properties. Moreover, the simplicity, scalability and the good control of the final CN composition will open many opportunities for the utilization of CN in (photo)electronic devices.

4. Experimental section

4.1 Synthesis of catalysts. Melamine needle-shaped crystals (M-nsc) were prepared by dissolving 150 mg of melamine in 50 ml of a water/HCl 37% (2% v/v) solution. As a result of the slow evaporation of the solvent, transparent needle-shaped crystals were obtained. In order to achieve CN materials, crystals were calcined at different temperatures (500, 600 and 650ºC) for 4h under an inert nitrogen atmosphere. Carbon doped crystals where synthetized by mixing 150 mg of melamine with 11.2 (5%), 22.5 (10%) and 45 mg (20%) of Benzoguanamine (2, 4-diamino-6-phenyl-1, 3, 5-triazine), BGA, in 50 ml of an aqueous solution acidified with HCl 37% (2% v/v). Transparent needle-shaped crystals were obtained by slow evaporation of the solvent and then calcined at 500 ºC for 4h under an inert nitrogen atmosphere (M-BGA).

4.2 Characterization. X-ray diffraction patterns were measured on a Bruker D8 advance instrument using Cu Kα radiation. Single Crystal XRD analysis was performed in a Bruker kappa APEXII Diffractometer. Nitrogen sorption measurements were taken with N_2 at 77 K after the samples had been degassed at 150 °C in vacuum for 20 h, using a Quantachrome Quadrasorb SI porosimeter. The apparent surface area of the final CN products was calculated

by applying the Brunauer-Emmett-Teller (BET) model to the isotherm data points of the adsorption branch. Elemental analysis was accomplished as combustion analysis using a Vario Micro device. HRSEM and TEM images were recorded on a JSM-7400F (JEOL) and Tecnai 12 TWIN instruments respectively. FT-IR spectra were recorded on a FTIR Spectrometer 6700. Optical absorbance spectra were measured using a Varian Spectrophotometer equipped with an integrating sphere, fluorescence measurements were performed using a FLS920P Spectrofluorimeter. Mass-loss data were obtained in a Thermogravimetric Analyzer Q500. The XPS data were collected by using an X-ray photoelectron spectrometer ESCALAB 250 ultrahigh vacuum (1×10-9 bar) apparatus with an AlKα X-ray source and a monochromator. The X-ray beam size was 500 μm and survey spectra was recorded with a pass energy (PE) of 150 eV and high energy resolution spectra were recorded with a PE of 20 eV. To correct for charging effects, all spectra were calibrated relative to a carbon C 1s peak, positioned at 284.8 eV. The XPS results were processed by using the AVANTGE software.. The apparent quantum yield (AQY) for H_2 evolution was determined by LEDs equipped with 420 and 490 nm band-pass filter. The irradiation area was 9 cm^2, and the irradiation intensity was measured by averaging 10 points in the irradiation area. The average intensity of 420 nm monochromatic light was 9.1 mW cm^{-2} and of 490 nm was 14 mW cm^{-2} (Newport 2936-R). The AQY was calculated as follows: AQY = Ne/Np × 100% = 2M/ Np × 100%, where N_e is the amount of reaction electrons, N_p is the incident photons, and M is the amount of H_2 molecules. The photocatalytic activity was further evaluated by the degradation of Rhodamine B (RhB) under white light irradiation. In a typical photocatalytic degradation experiment, RhB solution (20 ml, 20 mgL^{-1}) and carbon nitride (20 mg) were mixed in a glass vial in darkness with continuous stirring until the adsorption-desorption equilibrium between the dye and the catalyst was obtained. After turning on the light, aliquots were withdrawn from the suspension at given time intervals. The concentration of remaining RhB in solution was spectrophotometrically monitored by optical absorption values (at 554 nm of UV-vis absorption) on an ultraviolet-

visible spectrophotometer during the photodegradation process. Electrochemical measurements were recorded using a three-electrode system on an Autolab potentiostat (Metrohm, PGSTAT 101). A Pt foil electrode and an Ag/AgCl (3M KCl) electrode were used as the counter and reference electrode, respectively. Mott-Schottky ($1/C^2$ vs V) measurements were carried out in 1 M Na_2SO_4 aqueous solution as the electrolyte at a frequency of 2.48 kHz. Conductivity measurements of the CN materials were performed by the two contacts method (Scheme S1). CN is contacted with graphite ink between two Tungsten tips and a voltage between -10V and +10V is applied at room temperature. Electric current values are collected and a curve *I/V* is obtained, along the physical parameters of the CN needles and Ohms Law ($V = IR$), where I (A) is intensity and R (Ω) is resistance, we can calculate the value of the electric conductivity. The resistance ($R = (I/V)^{-1}$ Ω) depends on geometric parameters of the sample, then the value is expressed as resistivity $\rho = R(S/L)$, where S is the transversal section of the sample and L is the distance between the two contact points, due to the cylindrical shape of the CN materials and in order to simplify the measurement, both contributions of the transversal section (A, E, Scheme S1) share the same value. S and L values were obtained by comparison with an Atomic Force Microscopy cantilever of 200 µm long. Conductivity measurements ($\sigma = \rho^{-1}$ (S cm^{-1})) where performed by measuring several needles of the same sample and obtaining an average value.

Supporting Information

Supporting Information is available from the Wiley Online Library or from the author.

Acknowledgements

The authors thank financial support from the Spanish Ministerio de Economía y Competitividad (MAT2016-75883-C2-2-P…). We thank Dr. Hod for fruitful discussion.

Received: ((will be filled in by the editorial staff))
Revised: ((will be filled in by the editorial staff))
Published online: ((will be filled in by the editorial staff))

References

1. L. X. Zheng, M. J. O'connell, S. K. Doorn, X. Z. Liao, Y. H. Zhao, E. A. Akhadov, M. A. Hoffbauer, B. J. Roop, Q. X. Jia, R. C. Dye, D. E. Peterson, S. M. Huang, J. Liu, Y. T. Zhu, *Nat. Mater*. **2004**, *3*, 673-676.
2. R. Zhang, Q. Wen, W. Qian, D. S. Su, Q. Zhang, F. Wei, *Adv. Mater.* **2011**, *23*, 3387-3391.
3. R. Zhang, Z. Ning, Y. Zhang, Q. Zheng, Q. Chen, H. Xie, Q. Zhang, W. Qian, F. Wei, *Nat. Nanotechnol.* **2013**, *8*, 912-916.
4. B. C. Zhang, H. Wang, L. He, C. J. Zheng, J. S. Jie, Y. Lifshitz, S. T. Lee, X. H. Zhang, *Nano Lett.* **2017***, 17,* 7323-7329.
5. Y. Xia, P. Yang, Y. Sun, Y. Wu, B. Mayers, B. Gates, Y. Yin, F. Kim, H. Yan, *Adv. Mater.* **2003**, *15*, 353-389.
6. F.-X. Xiao, J. Miao, H. B. Tao, S.-F. Hung, H.-Y. Wang, H. B. Yang, J. Chen, R. Chen, B. Liu, *Small* **2015**, *11*, 2115-2131.
7. Z. Lai, Y. Chen, C. Tan, X. Zhang, H. Zhang, *Chem* **2016**, *1*, 59-77.
8. J. Tian, Z. Zhao, A. Kumar, R. I. Boughton, H. Liu, *Chem. Soc. Rev.* **2014**, *43*, 6920-6937.
9. J. Qu, C. Lai *J. Nanomater.* **2013**, *2013,* 1-11.

10. Z. Chen, J. Appenzeller, Y. M. Lin, J. Sippel-Oakley, A. G. Rinzler, *Science* **2006***, 311,* 1735-1735.

11. W. Park, G. Zheng, X. Jiang, B. Tian, C. M. Lieber *Nano Lett.* **2008,** *8,* 3004-3009.

12. M. Ge, Q. Li, C. Cao, J. Huang, S. Li, S. Zhang, Z. Chen, K. Zhang, S. S. Al-Deyab, Y. Lai. *Adv. Sci.* **2017**, *4*, 1600152-1600183.

13. B. Weng, S. Liu, Z. R. Tang, Y. J. Xu, *RSC Adv.* **2014**, *4*, 12685-12700.

14. X. Wang, K. Maeda, A. Thomas, K. Takanabe, G. Xin, J. M. Carlsson, K. Domen, M. Antonietti, *Nat. Mater.* **2009**, *8*, 76-80.

15. A. Thomas, A. Fischer, F. Goettmann, M. Antonietti, J.-O. Müller, R. Schlögl, J. M. Carlsson, *J. Mater. Chem.* **2008**, *18*, 4893.

16. J. Zhu, P. Xiao, H. Li, S. A. Carabineiro, *ACS Appl. Mater Interfaces* **2014**, *6*, 16449-16465.

17. Y. Zheng, J. Liu, J. Liang, M. Jaroniec, S. Z. Qiao, *Energy Environ. Sci.* **2012**, *5*, 6717.

18. W. J. Ong, L. L. Tan, Y. H. Ng, S. T. Yong, S. P. Chai, *Chem. Rev.* **2016**, *116*, 7159-7329.

19. J. Xu, T. J. Brenner, Z. Chen, D. Neher, M. Antonietti, M. Shalom, *ACS Appl. Mater. Interfaces* **2014**, *6*, 16481-16486.

20. G. Dong, L. Zhang, *J. Mater. Chem.* **2012**, *22*, 1160-1166.

21. M. Shalom, S. Gimenez, F. Schipper, I. Herraiz-Cardona, J. Bisquert, M. Antonietti, *Angew. Chem. Int. Ed.* **2014**, *53*, 1-6.

22. J. Albero, E. M. Barea, J. Xu, I. Mora-Seró, H. Garcia, M. Shalom, *Adv. Mater. Interfaces* **2017**, *4*, 1600265.

23. Y. Wang, X. Wang, M. Antonietti, *Angew. Chem. Int. Ed.* **2012**, *51*, 68-89.

24. J. Lin, Z. Pan, X. Wang, *ACS Sustain. Chem. Eng.* **2014**, *2*, 353-358

25. X. Wang, K. Maeda, X. Chen, K. Takanabe, K. Domen, Y. Hou, X. Fu, M. Antonietti, *J. Am. Chem. Soc.* **2009**, *131*, 1680-1681.

26. X. Yang, H. Tang, J. Xu, M. Antonietti, M. Shalom, *ChemSusChem* **2015**, *8*, 1350-1358.

27. G. Zhang, Z.-A. Lan, L. Lin, S. Lin, X. Wang, *Chem. Sci.* **2016**, *7*, 3062-3066.

28. J. Xu, M. Shalom, F. Piersimoni, M. Antonietti, D. Neher, T. J. K. Brenner, *Adv. Opt. Mater.* **2015**, *3*, 913-917

29. J. Xu, T. J. K. Brenner, L. Chabanne, D. Neher, M. Antonietti, M. Shalom, *J. Am. Chem.Soci.* **2014**, *136*, 13486-13489.

30. J. Xu, I. Herraiz-Cardona, X. Yang, S. Gimenez, M. Antonietti, M. Shalom, *Adv. Opt. Mater.* **2015**, *3*, 1052-1058.

31. Y. Wang, J. Zhang, X. Wang, M. Antonietti, H. Li, *Angew. Chem. Int. Ed.* **2010**, *49*, 3356-3359.

32. Y. Zhang, T. Mori, J. Ye, M. Antonietti, *J. Am. Chem. Soc.* **2010**, *132*, 6294-6295.

33. L. Jiang, X. Yuan, Y. Pan, J. Liang, G. Zeng, Z. Wu, H. Wang, *Appl. Catal. B* **2017**, *217*, 388-406.

34. Q. Cui, J. Xu, X. Wang, L. Li, M. Antonietti, M. Shalom, *Angew. Chem. Int. Ed.* **2016**, *55*, 3672-3676.

35. S. Yang, Y. Gong, J. Zhang, L. Zhan, L. Ma, Z. Fang, R. Vajtai, X. Wang, P. M. Ajayan, *Adv. Mater.* **2013**, *25*, 2452-2456.

36. J. Xu, L. Zhang, R. Shi, Y. Zhu, *J.Mater Chem. A* **2013**, *1*, 14766-14772.

37. Z. Yang, Y. Zhang, Z. Schnepp, *J.Mater. Chem. A* **2015**, *3*, 14081-14092.

38. F. Goettmann, A. Fischer, M. Antonietti, A. Thomas, *Angew. Chem. Int. Ed.* **2006**, *45*, 4467-4471.

39. M. Shalom, S. Inal, C. Fettkenhauer, D. Neher, M. Antonietti, *J. Am. Chem. Soc.* **2013**, *135*, 7118-7121.

40. Y.-S. Jun, E. Z. Lee, X. Wang, W. H. Hong, G. D. Stucky, A. Thomas, *Adv. Funct. Mater.* **2013**, *23*, 3661-3667.

41. G. Peng, L. Xing, J. Barrio, M. Volokh, M. Shalom, *Angew. Chem. Int. Ed.* **2018**, *130*, 1200-1206.

42. M. Shalom, M. Guttentag, C. Fettkenhauer, S. Inal, D. Neher, A. Llobet, M. Antonietti, *Chem. Mater.* **2014**, *26*, 5812-5818.

43. J. Barrio, L. Lin, X. Wang, M. Shalom, *ACS Sustain. Chem. Eng.* **2018**, *6*, 519-530.

44. J. Barrio, M. Shalom, *Mater. Sci. Semicond. Process.* **2018**, *73*, 78-82.

45. L. Li, M. Shalom, Y. Zhao, J. Barrio, M. Antonietti, *J. Mater. Chem. A* **2017**, *5*, 18502-18508.

46. J. Liu, J. Huang, H. Zhou, M. Antonietti, *ACS Appl. Mater. Interfaces* **2014**, *6*, 8434-8440.

47. H. J. Li, D. J. Qian, M. Chen, *ACS Appl. Mater. Interfaces* **2015**, *7*, 25162-25170.

48. Y. Zhao, Z. Liu, W. Chu, L. Song, Z. Zhang, D. Yu, Y. Tian, S. Xie, L. Sun, *Adv. Mater.* **2008**, *20*, 1777-1781.

49. M. Tahir, C. Cao, N. Mahmood, F. K. Butt, A. Mahmood, F. Idrees, S. Hussain, M. Tanveer, Z. Ali, I. Aslam, *ACS Appl. Mater. Interfaces* **2014**, *6*, 1258-1265.

50. J. Janczak, G. J. Perpetuo, *Acta Cryst. C* **2001**, *57*, 1120-1122.

51. M. K. Marchewka, *Mat. Sci. Eng., B* **2002**, *95*, 214-221.

52. A. B. Koren, M. D. Curtis, A. H. Francis, J. W. Kampf, *J. Am. Chem Soc.* **2003**, *125*, 5040-5050.

53. W. Tu, Y. Xu, J. Wang, B. Zhang, T. Zhou, S. Yin, S. Wu, C. Li, Y. Huang, Y. Zhou, Z. Zou, J. Robertson, M. Kraft, R. Xu, *ACS Sustain. Chem. Eng* **2017**, *5*, 7260-7268.

54. P. Niu, G. Liu, H.-M. Cheng, *J. Phys. Chem. C* **2012**, *116*, 11013-11018.

55. P. Niu, L.-C. Yin, Y.-Q. Yang, G. Liu, H.-M. Cheng, *Adv. Mater.* **2014**, *26*, 8046-8052.

56. J. Bian, L. Xi, J. Li, Z. Xiong, C. Huang, K. M. Lange, J. Tang, M. Shalom, R.-Q. Zhang, *Chem. Asian J.* **2017**, *12*, 1005-1012.

57. T. Jordan, N. Fechler, J. Xu, T. J. K. Brenner, M. Antonietti, M. Shalom, *ChemCatChem* **2015**, *7*, 2826-2830

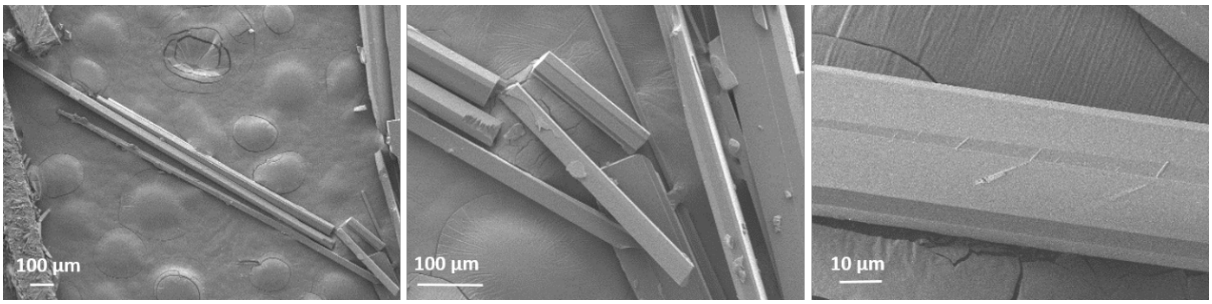

Figure 1. SEM Images of Melamine needle-shaped single crystal before calcination.

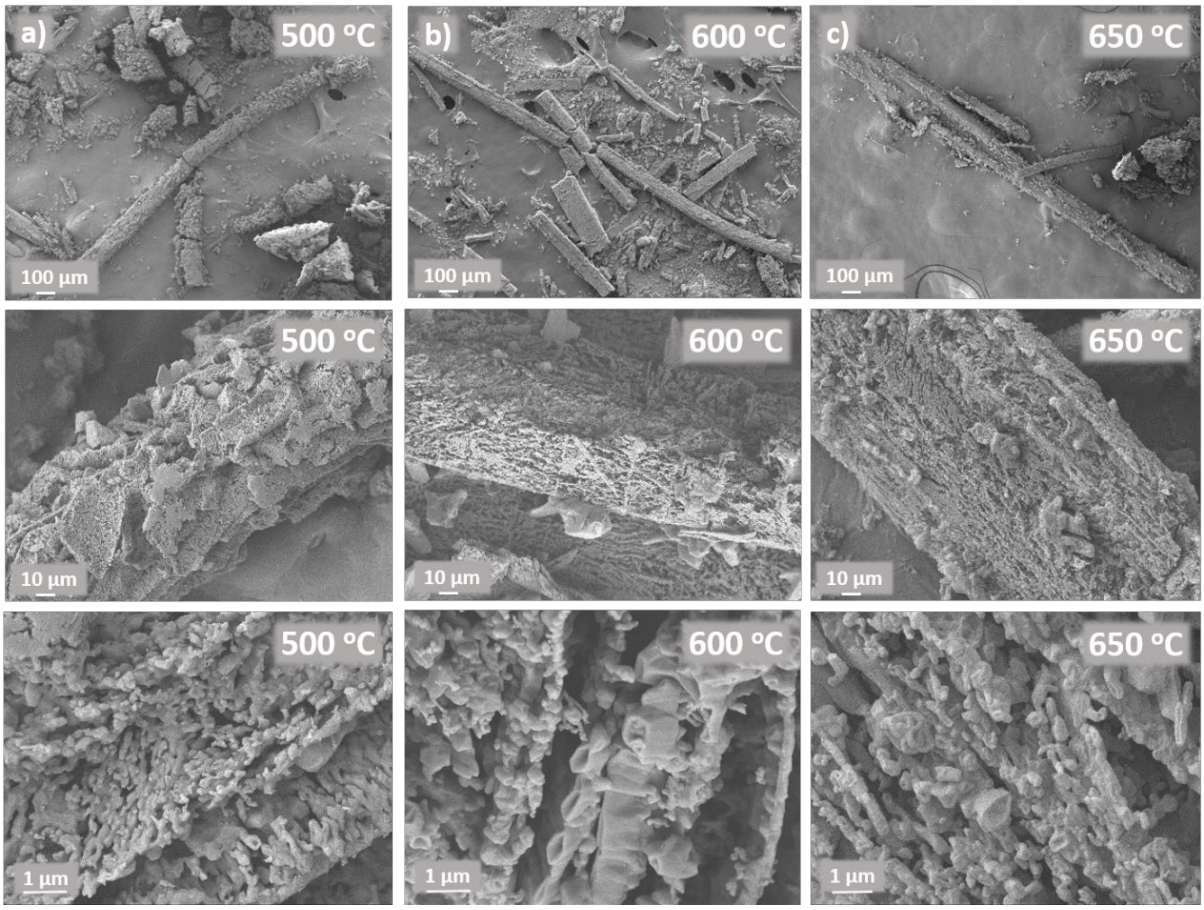

Figure 2. SEM images melamine needle-shaped crystal calcined at (a) 500 °C, (b) 600 °C and (c) 650 °C.

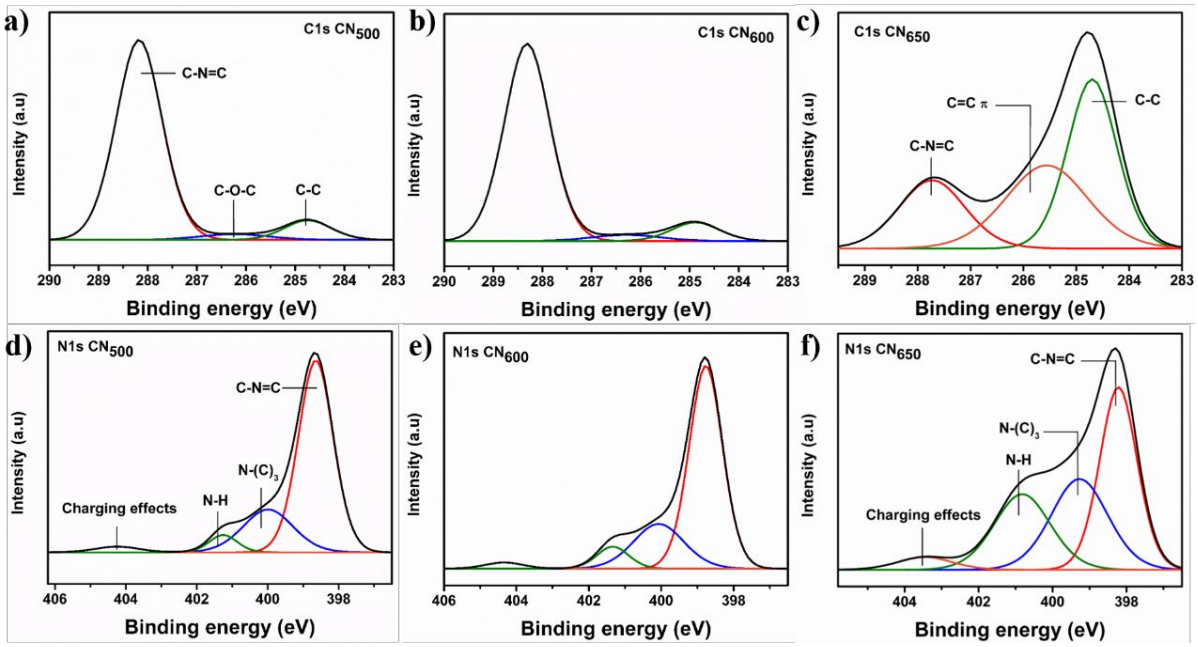

Figure 3. C1s and N1s XPS Spectra of CN_{500} (a, d), CN_{600} (b, e) and CN_{650} (c, f).

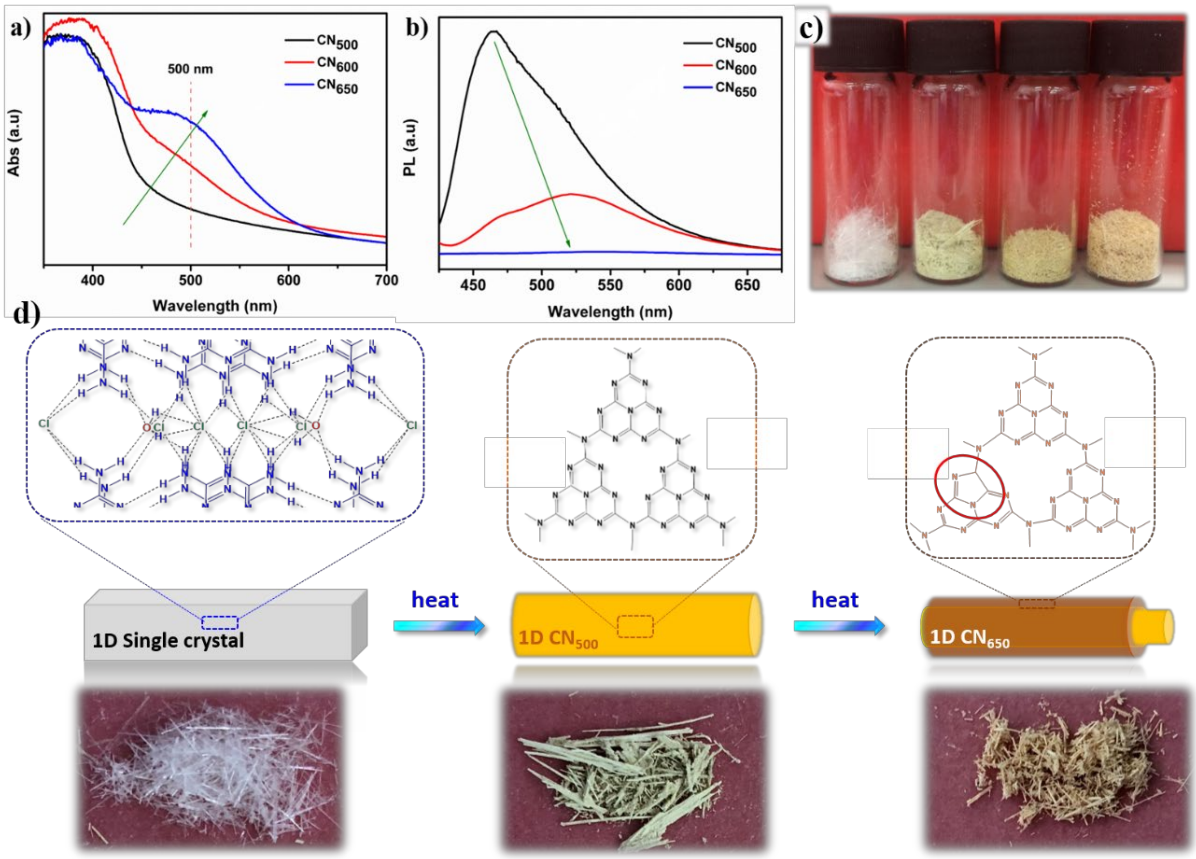

Figure 4. (a) UV-vis diffuse reflectance spectra and (b) emission spectra of the materials after calcination, (c) pictures of M-nsc, CN_{500}, CN_{600} and CN_{650} and (d) proposed structure of the materials before and after calcination at different temperatures.

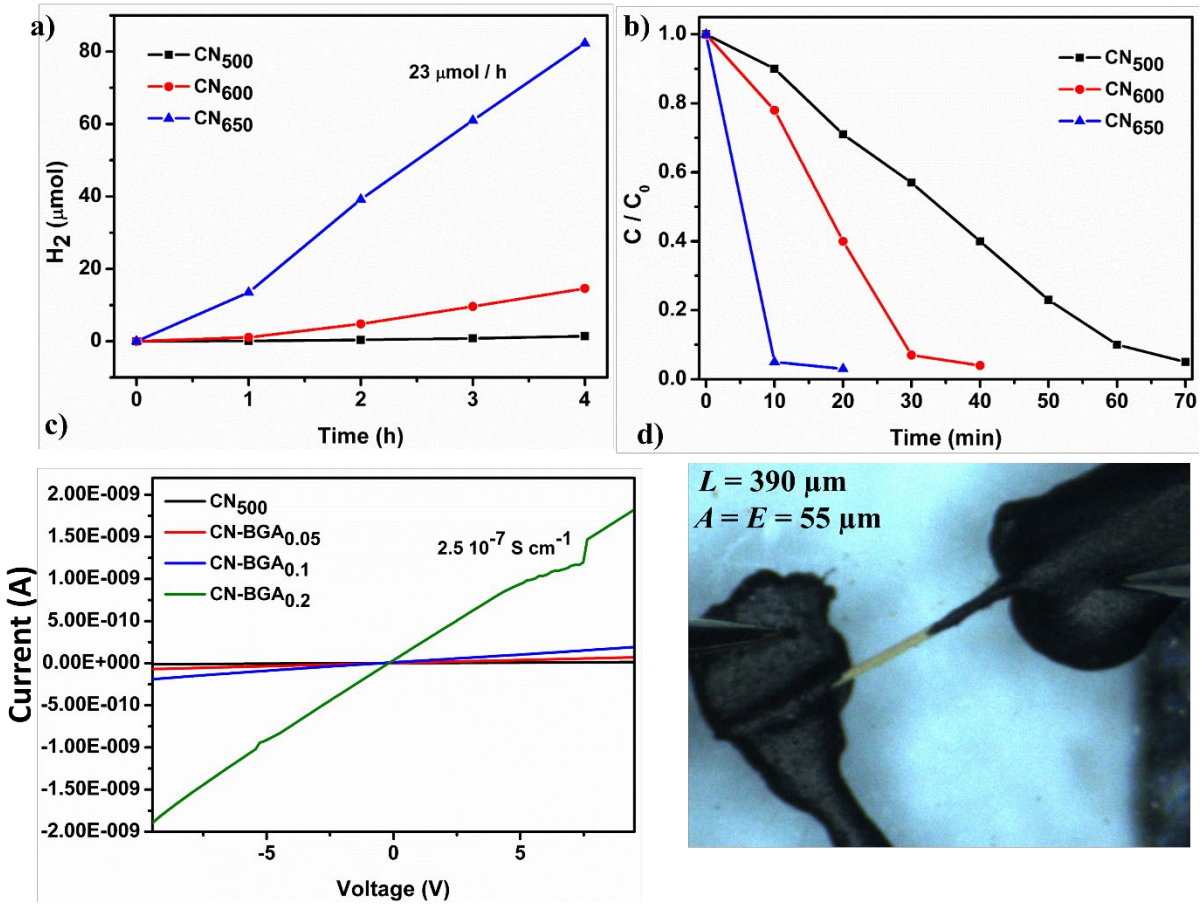

Figure 5. a) H_2 production values from water splitting of CN materials. b) Photochemical degradation curves of RhB dye with CN materials synthetized at different temperatures. c) Plot of I/V for CN_{500} and CN-BGA_x materials. d) Optical microscope image of a contacted needle corresponding to CN-$BGA_{0.2}$ along its dimensions.

Centimeter-long polymeric carbon nitride needles with tunable optical, electric and catalytic properties are synthesized by employing organic crystals as precursor. The ultralong CN needles allow the facile and direct measurements of their electronic conductivity while exhibiting good photocatalytic properties. The new growth strategy provides new opportunity for CN and other metal-free materials design toward their utilization in photoelectronic related devices.

Keywords: one-dimensional (1D) nanostructures, polymeric carbon nitride, direct electric measurements, photocatalysis

J. Barrio, L. Lin, P. Amo-Ochoa, J. Tzadikov, G. Peng, J. Sun, F. Zamora, X. Wang, M. Shalom *

Unprecedented Centimeter-long Carbon Nitride Needles: Synthesis, Characterization and Applications

ToC figure

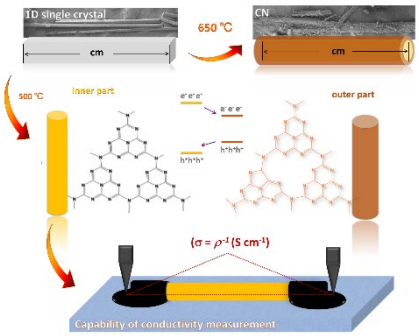

Supporting Information for:

Unprecedented Centimeter-long Carbon Nitride Needles: Synthesis, Characterization and Applications

Jesús Barrio, [†] *Lihua Lin,* [¥] *Pilar Amo-Ochoa,* [‡] *Jonathan Tzadikov,* [†] *Guiming Peng,* [†] *Jingwen Sun,* [†] *Félix Zamora,* [‡§] *Xinchen Wang,* [¥] *Menny Shalom* [†]*

Jesús Barrio, Jonathan Tzadikov, Dr. Guiming Peng, Dr. Jingwen Sun, Prof. Menny Shalom.
† Department of Chemistry, Ben Gurion University of the Negev, Beersheba 009728, Israel
E-mail: mennysh@post.bgu.ac.il

Ling Lihua, Prof. Xinchen Wang.
¥ College of Chemistry, Fuzhou University, Gong Ye Road 523, Fuzhou, Fujian, Fuzhou 350002 P. R. China.

Dr. Pilar Amo-Ochoa, Dr. Félix Zamora.
‡ Departamento de Química Inorgánica, Institute for Advanced Research in Chemical Sciences (IAdChem) and Condensed Matter Physics Center (IFIMAC), Universiidad Autónoma de Madrid, E-28049 Madrid, Spain

§ Instituto Madrileño de Estudios Avanzados en Nanociencia (IMDEA-Nanociencia), Cantoblanco, E-28049 Madrid, Spain

Single Crystal XRD Analysis		
Chemical formula	$C_6H_{16}Cl_2N_{12}O$	
Formula weight	343.18	
Wavelength	0.71073Å	
Crystal habit	Clear colourless prismatic	
Crystal system	Monoclinic	
Unit cell dimensions	a = 12.419(7) Å b = 17.676(8) Å c = 7.072(3) Å	α = 90° β = 115.18(2)° γ = 90°
Volume	1405.0(11) Å	

Figure S1. Crystal data obtained by SC-XRD analysis.

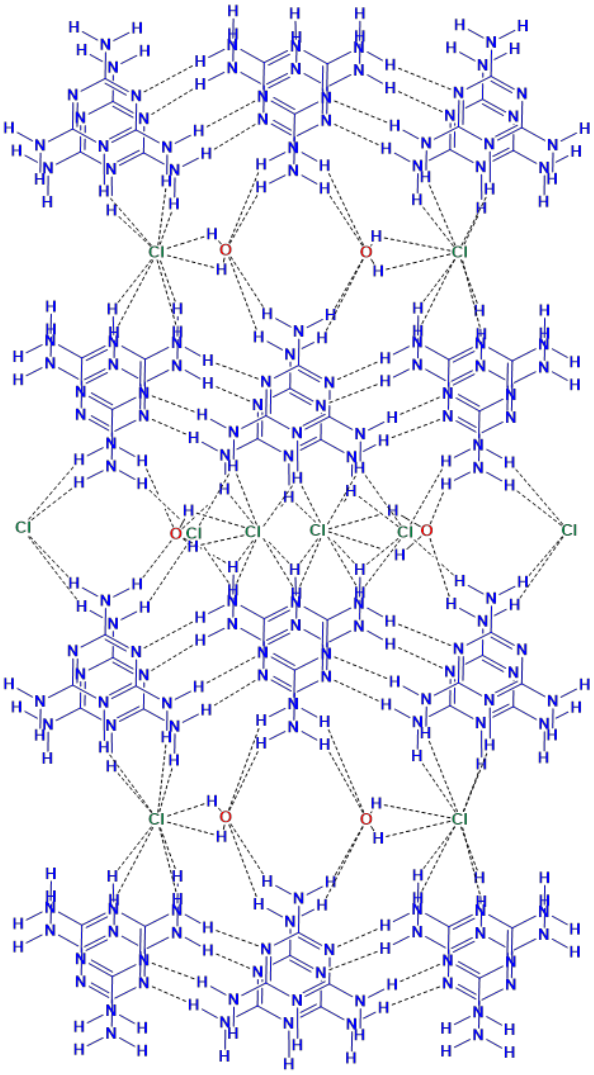

Figure S2. Molecular arrangement in the unit cell.

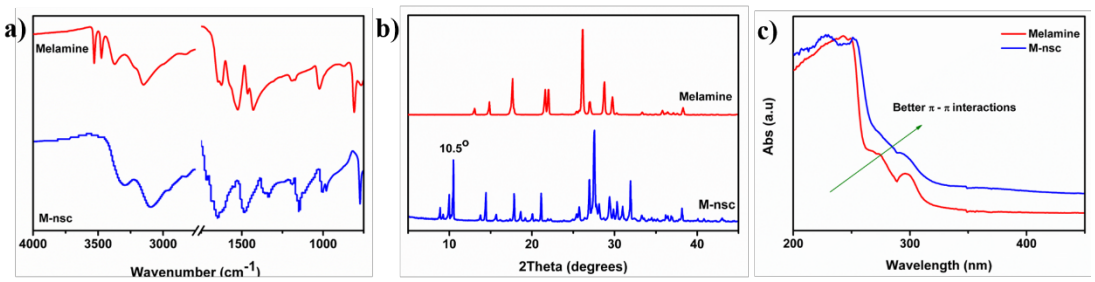

Figure S3. Melamine and melamine needle shaped crystal FT-IR Spectra (a), XRD patterns (b) and UV-vis spectra.

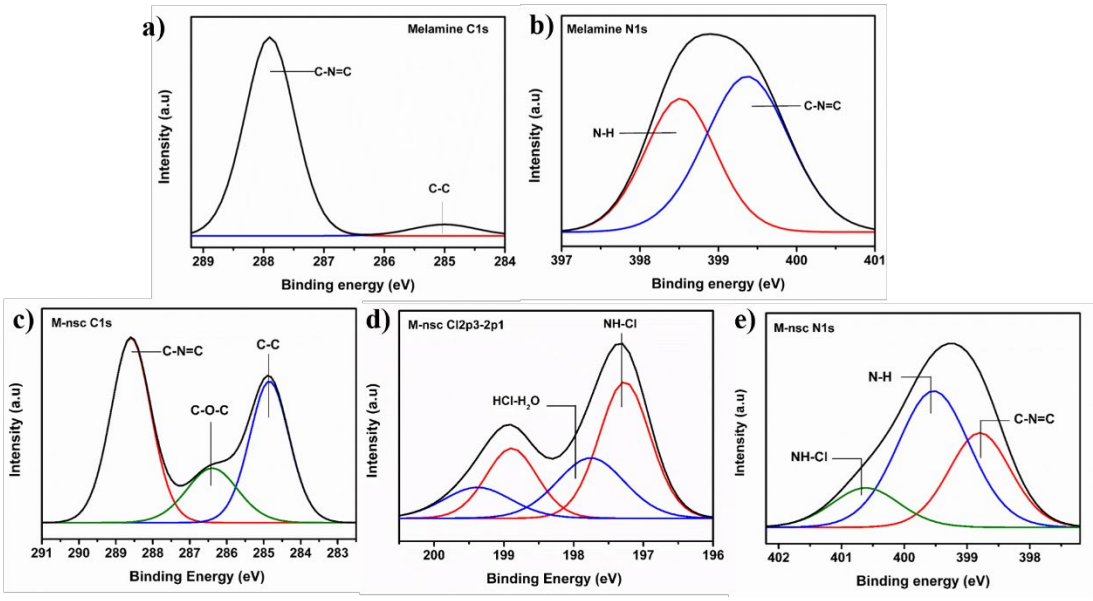

Figure S4. XPS analysis for melamine (a, b) and M-nsc (c-e).

The Cl 2p3, 2p1 XPS patterns reveal the presence of two different chemical states in the material at 197.27 Cl 2p3 – 198.89 Cl 2p1 and 197.76 Cl 2p3 – 199.38 Cl 2p1corresponding to a NH-Cl coordination and HCl.H2O. The formation of an arrangement is strongly reflected also in the N1s spectrum, shown in the presence of three different chemical states; C-N heterocycle (398.8 eV), amine type N (399.5 eV) and one more contribution at 400.6 eV which belongs to the NH-Cl coordination, meanwhile in melamine just two peaks are observed at 398.5 and 399.4 eV; C-N heterocycle and amine type N respectively. At C1s spectra, the contributions shown belong to C-C and C-O adventitious bonds (284.8-286.4 eV, respectively) and the C-N specie corresponding the Melamine heterocycle at 288.6 eV. For melamine, just C-N from the heterocycle and adventitious C-C are observed at 284.9 and 288.0 respectively.

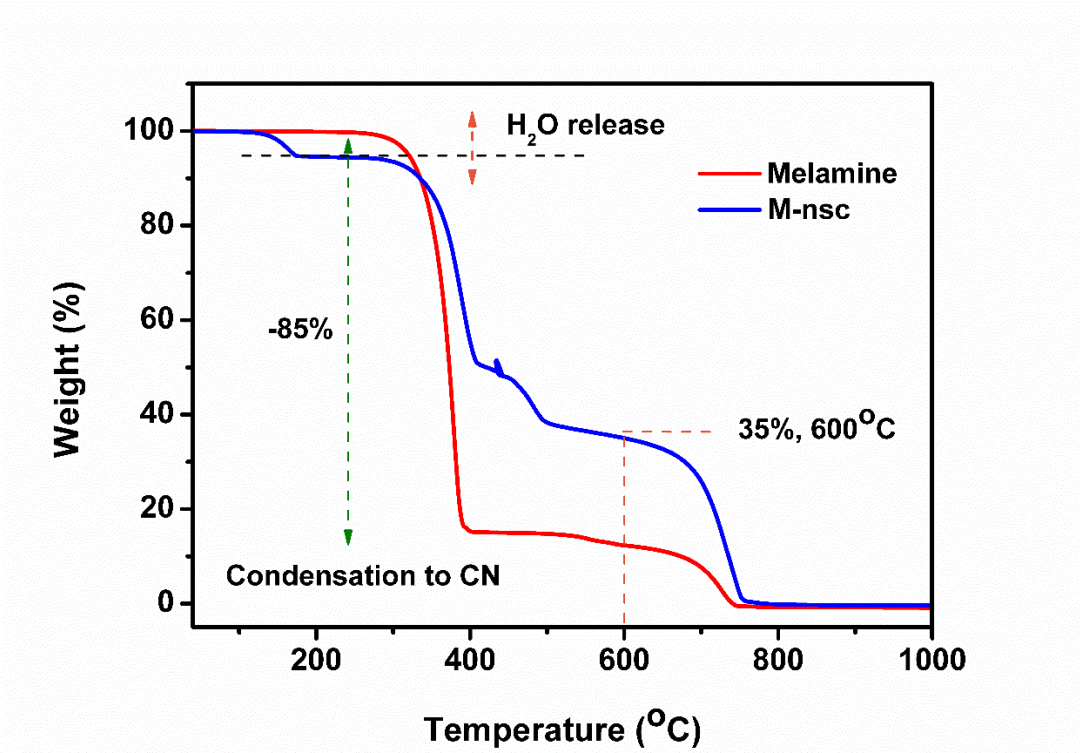

Figure S5. Thermal gravimetric analysis of melamine and M-nsc.

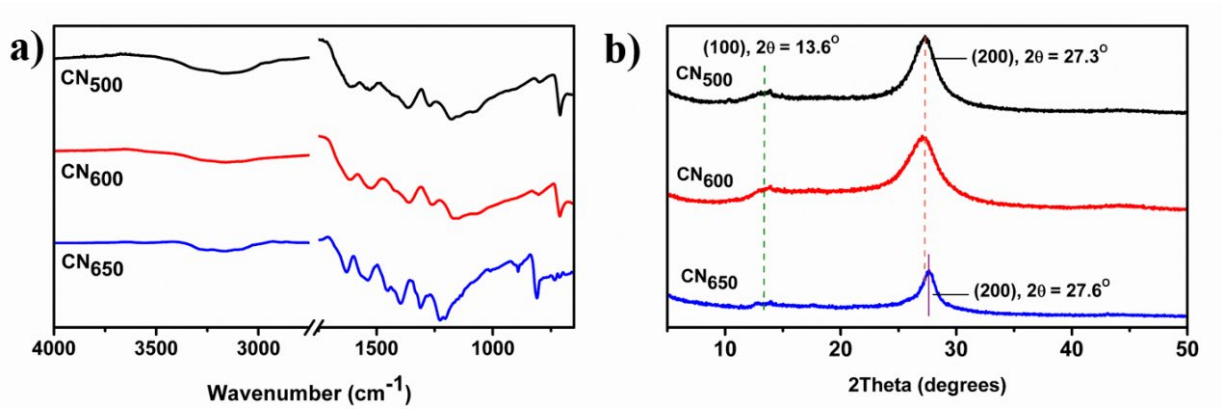

Figure S6. FT-IR Spectra (a) and XRD patterns (b) of CN_{500}, CN_{500} and CN_{650}.

Sample	N%	C%	H%	C/N ratio
CN_{500}	57.02	32.07	2.07	0.562
CN_{600}	56.03	31.72	2.03	0.565
CN_{650}	58.9	33.50	1.67	0.569

Table S1. Elemental analysis data of CN materials calcined at different temperatures.

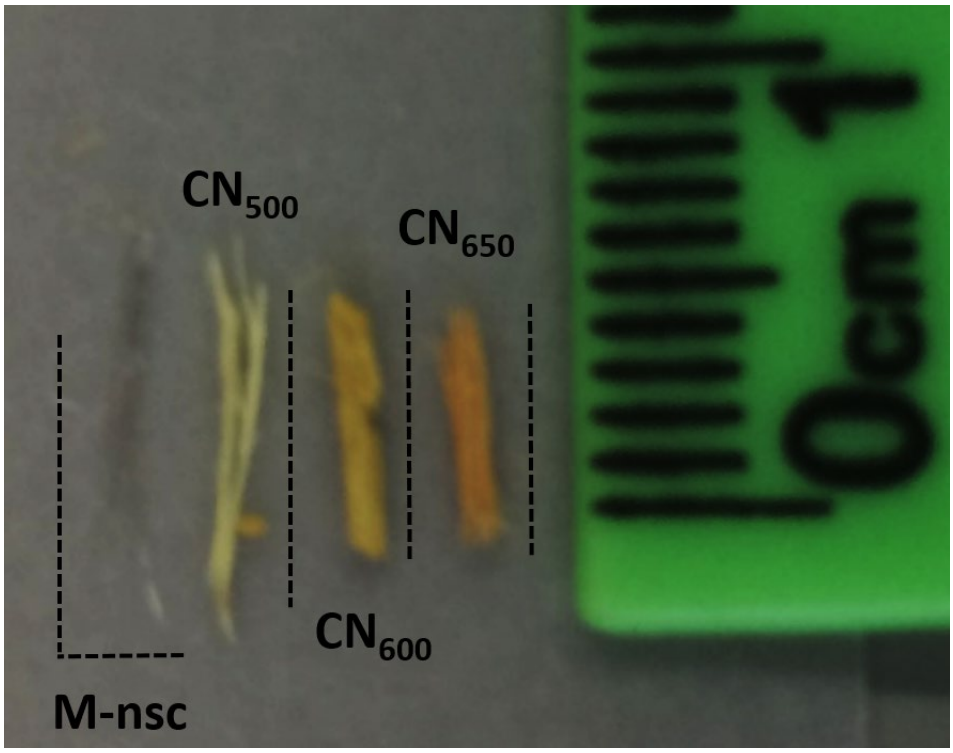

Figure S7. Pictures of M-nsc and CN materials

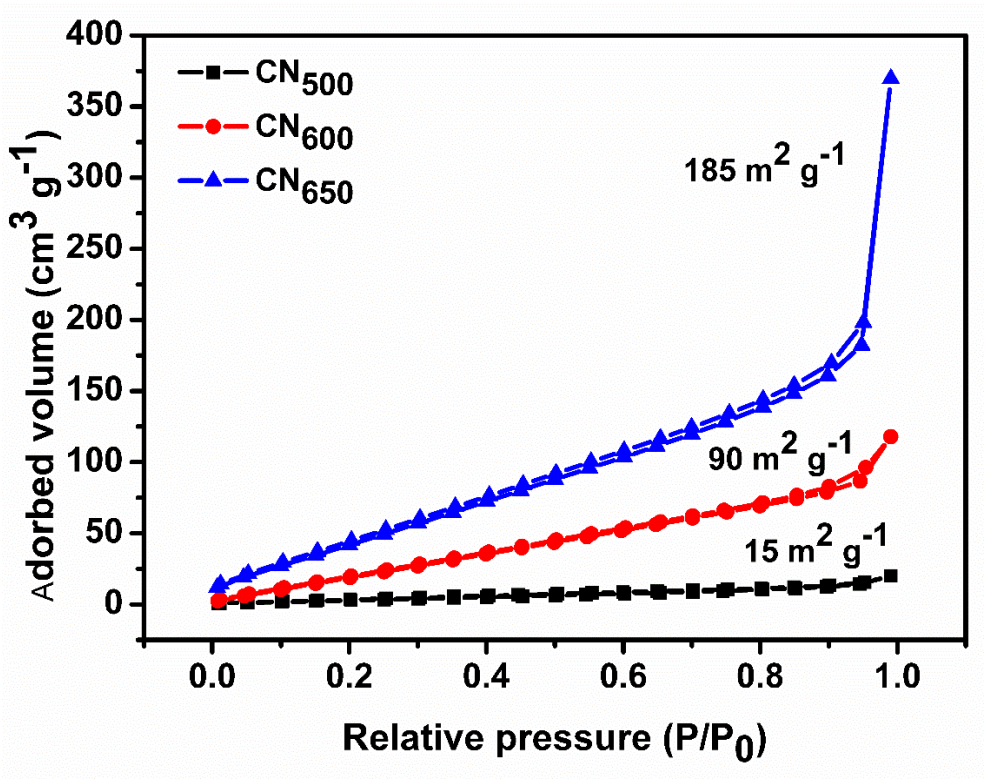

Figure S8. Nitrogen-sorption measurements of CN materials.

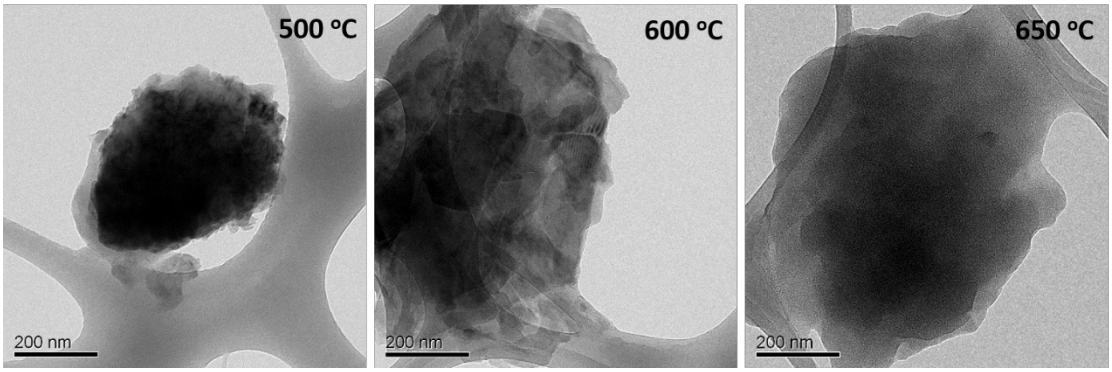

Figure S9. TEM images of exfoliated CN_{500}, CN_{600} and CN_{650}. For this experiment, a suspension of 0.3 mg/ml of the catalysts in water was exfoliated by simple ultrasonication for 10 hours in a water bath, followed by centrifugation to remove residual big aggregates resulting in colloidal suspensions with high transparency.

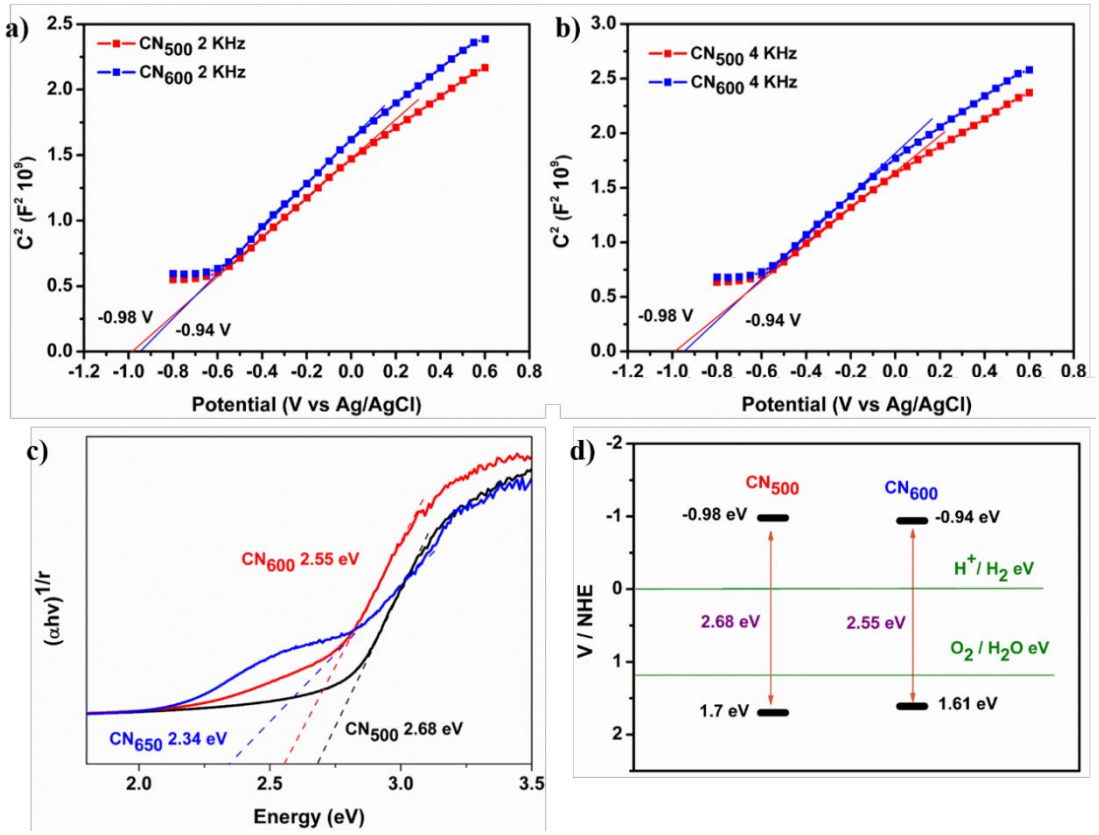

Figure S10. Mott-Schottky plots for CN_{500} and CN_{600} (a, b), (c) Tauc Plot of CN materials and (d) conduction and valence bands positions for CN_{500} and CN_{600}.

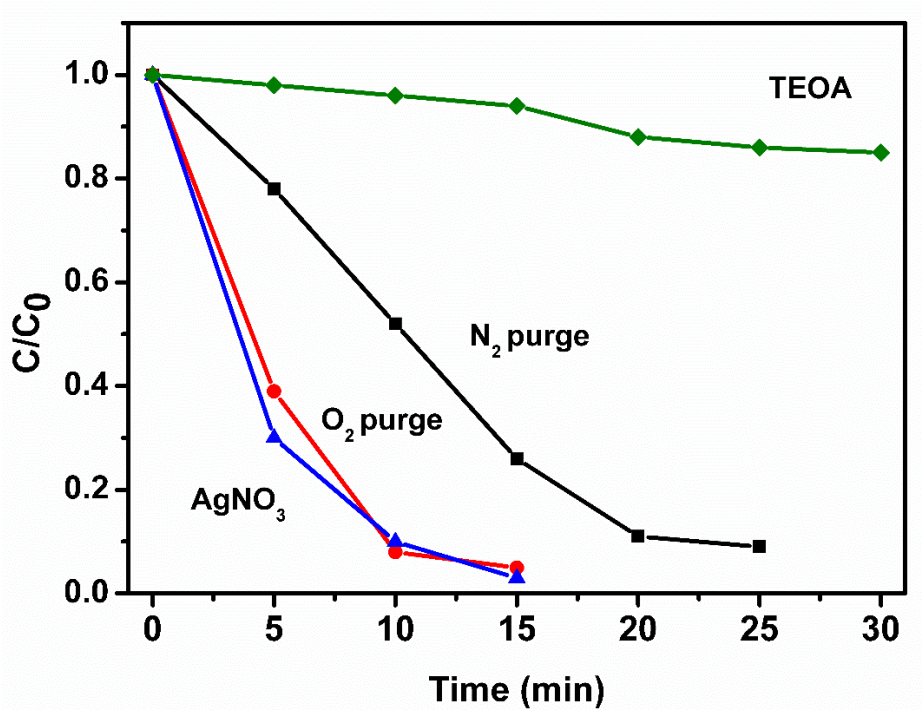

Figure S11. Comparison of RhB degradation with CN_{650} and different additives.

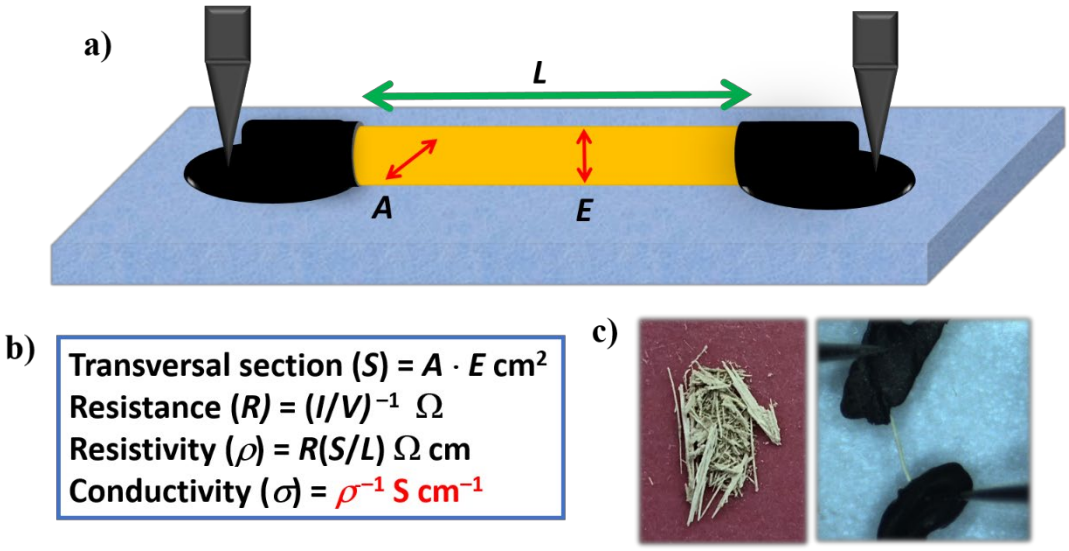

Scheme S1. Representation of electrical conductivity measurements methodology (a), calculations required in order to obtain conductivity values ($\sigma = \rho^{-1}$ (S cm^{-1})) of given samples (b) and optical pictures of the CN_{500} sample and a CN_{500} needle contacted with graphite ink and a Tungsten tips (c).

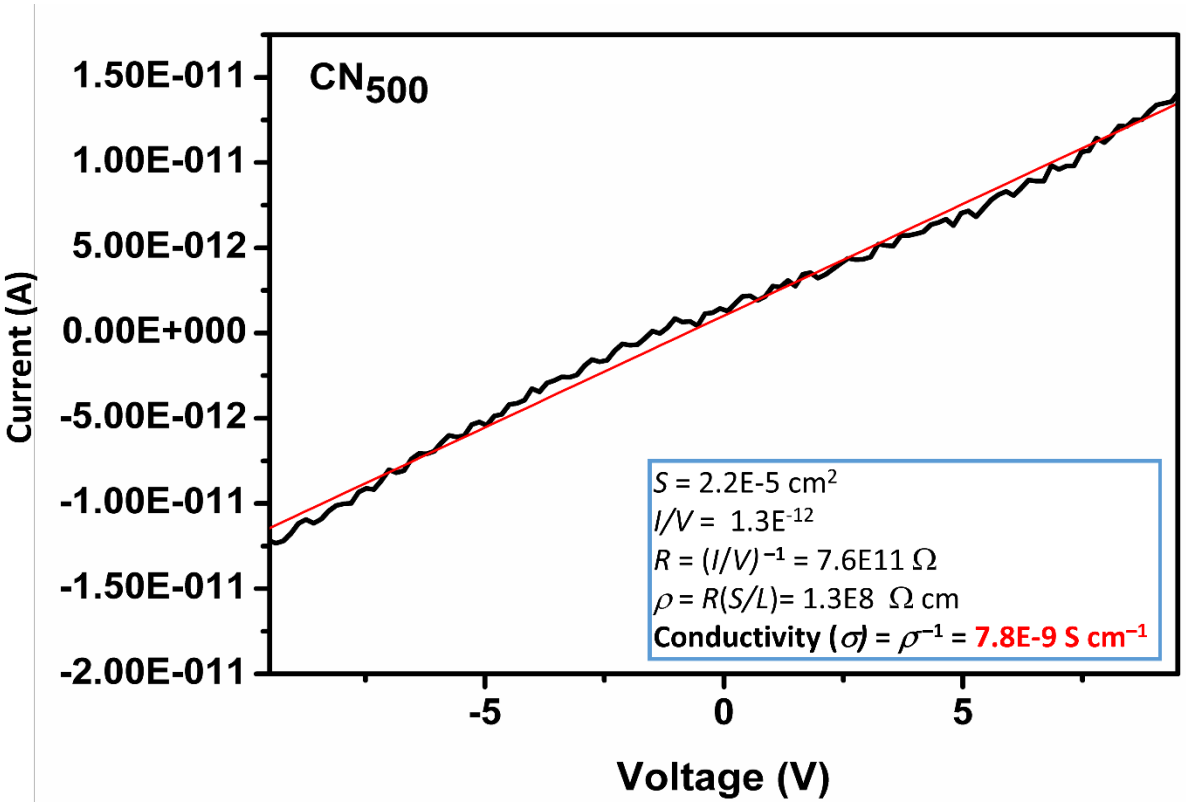

Figure S12. a) Plot of I/V and conductivity calculations for CN_{500}.

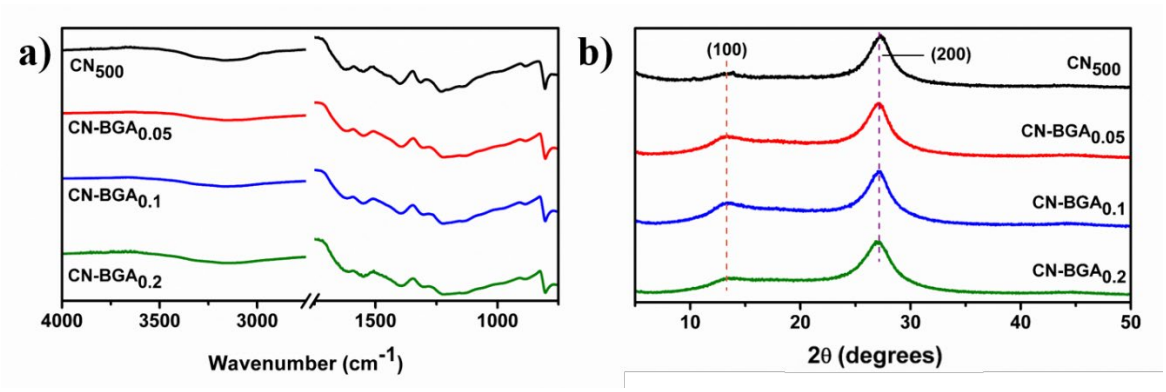

Figure S13. FTIR spectra (a) and XRD patterns (b) of C doped CN materials.

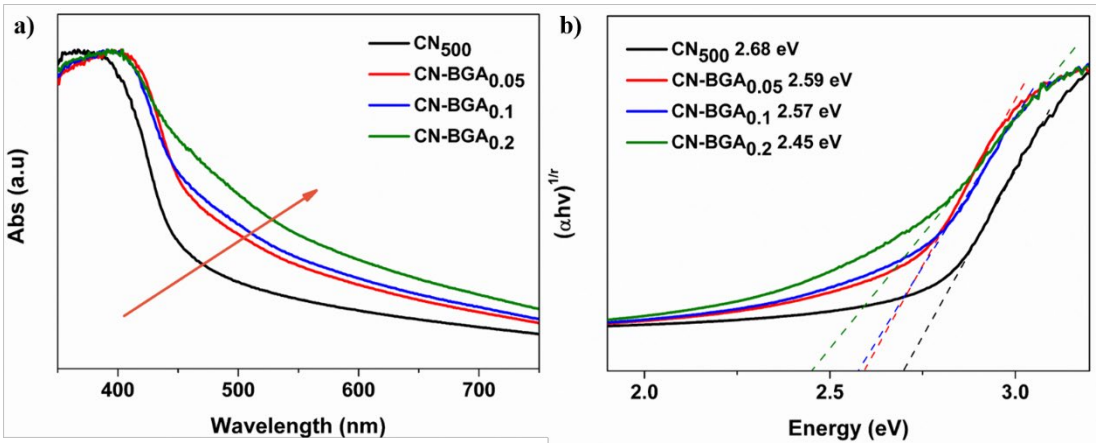

Figure S14. UV-Vis spectra (a) and Tau Plot (b) of C doped CN materials.

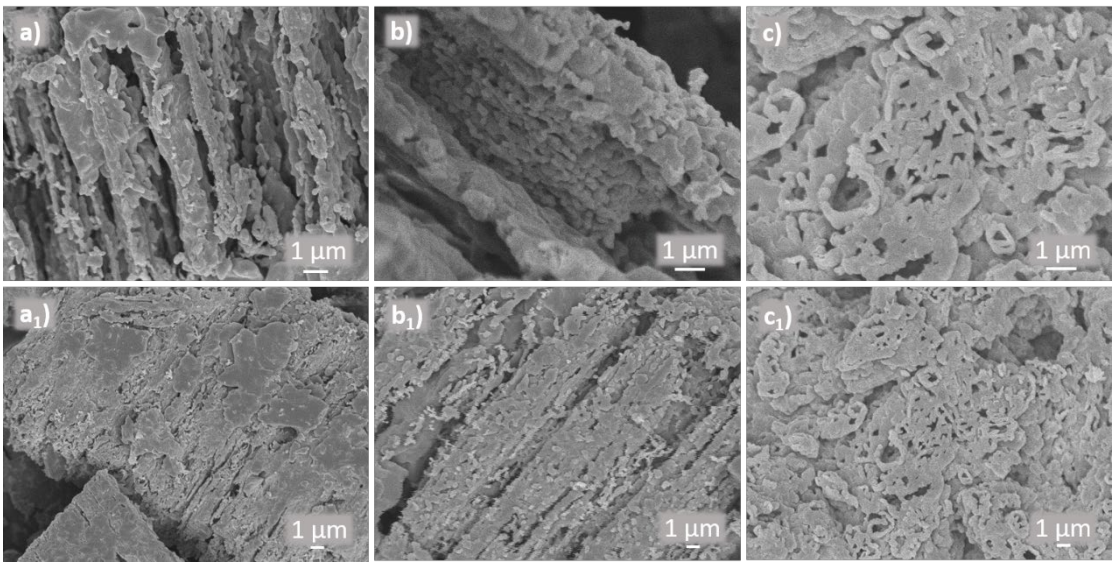

Figure S15. SEM pictures of (a) CN-BGA$_{0.05}$, (b) CN-BGA$_{0.1}$ and CN-BGA$_{0.2}$.